Sensors and Actuators B 262 (2018) 750–757

Contents lists available at ScienceDirect

Sensors and Actuators B: Chemical

journal homepage: www.elsevier.com/locate/snb

Biological hydrogen peroxide detection with aryl boronate and benzil BODIPY-based fluorescent probes

Malcolm S. Purdey[a,b,c,d], Hanna J. McLennan[a,b,e], Melanie L. Sutton-McDowall[a,b,e], Daniel W. Drumm[a,f], Xiaozhou Zhang[a,b,c], Patrick K. Capon[a,b,c], Sabrina Heng[a,b,c,*], Jeremy G. Thompson[a,b,e], Andrew D. Abell[a,b,c]

[a] ARC Centre of Excellence for Nanoscale BioPhotonics (CNBP), Australia
[b] Institute for Photonics and Advanced Sensing (IPAS), The University of Adelaide, North Terrace, Adelaide, SA, 5005, Australia
[c] Department of Chemistry, School of Physical Sciences, The University of Adelaide, North Terrace, Adelaide, SA, 5005, Australia
[d] South Australian Health and Medical Research Institute (SAHMRI) and School of Medicine, Adelaide Medical School, Faculty of Health and Medical Sciences, North Terrace, Adelaide, SA, 5001, Australia
[e] Robinson Research Institute and School of Medicine, Faculty of Health Sciences, Adelaide Medical School, Faculty of Health and Medical Sciences The University of Adelaide, North Terrace, Adelaide, SA, 5005, Australia
[f] Australian Research Council Centre of Excellence for Nanoscale BioPhotonics, School of Sciences, RMIT University, Melbourne, Vic, 3001, Australia

ARTICLE INFO

Article history:
Received 26 September 2017
Received in revised form 18 January 2018
Accepted 25 January 2018
Available online 31 January 2018

Keywords:
Fluorescent sensor
Hydrogen peroxide
BODIPY
Reactive oxygen species

ABSTRACT

The detection of hydrogen peroxide (H_2O_2) using fluorescent probes is critical to the study of oxidative stress in biological environments. Two important sensing architectures for detecting H_2O_2, aryl boronates and benzils, are compared here using novel boron-dipyrromethene (BODIPY) fluorescent probes. The aryl boronate PeroxyBODIPY-1 (**PB1**) and benzil-based nitrobenzoylBODIPY (**NbzB**) were synthesised from a common BODIPY intermediate in order to compare sensitivity and selectivity to H_2O_2. The aryl boronate **PB1** gives the highest change in fluorescence on reaction with H_2O_2 while the benzil **NbzB** exhibits exclusive selectivity for H_2O_2 over other reactive oxygen species (ROS). Both proved to be cell-permeable, with **PB1** being able to detect H_2O_2 in denuded bovine oocytes. The strengths of these aryl boronate and benzil probes can now be exploited concurrently to elucidate biological mechanisms of H_2O_2 production and oxidative stress.

1. Introduction

Hydrogen peroxide (H_2O_2) is an important reactive oxygen species (ROS) that acts as both a cellular signaller [1] and a causative of oxidative stress [2]. Such cellular stress can have serious consequences for cell function, *e.g.* it results in defective sperm function [3] and compromised embryonic development in reproductive biology [4]. The detection of H_2O_2 is thus of real importance in understanding both the mechanisms of oxidative stress and a range of cellular signalling processes.

More specifically, fluorescent probes are commonly used for *in situ* detection of H_2O_2 and real-time monitoring of associated processes within an oocyte or embryo [5,6]. These fluorophores function by giving a measurable change in fluorescence on reaction with H_2O_2. While many fluorescent probes for H_2O_2 (*e.g.* 2′,7′-dichlorohydrofluorescein diacetate) [7] suffer from a lack of specificity for H_2O_2 over other biologically relevant ROS, fluorescent probes bearing the aryl boronates [7–9] and benzyl reactive groups are known to exhibit selectivity for H_2O_2 (see Fig. 1**A** and **B** for reaction mechanisms) [10,11] and are important as they provide an opportunity to elucidate the identity of specific oxidants in biological production of ROS [12]. Unlike many fluorescent probes (e.g. 2′,7′-dichlorohydrofluoresceindiacetate), [7] aryl boronates [7–9] andbenzil-based systems exhibit good selectivity for H_2O_2 over other biologically relevant ROS (see Fig. 1A and B for reaction mechanisms). [10,11] These probes thus provide an opportunity to help identify specific oxidants involved in the biological production of ROS [12].

An experimental comparison of the ability of aryl boronate and benzil fluorescent probes to detect H_2O_2 is required, as comparative strengths and weaknesses of each probe is critical to understand the role of H_2O_2 in biological processes. A peroxide based probe should have the following criteria to be useful in biological applications. In

* Corresponding author at: ARC Centre of Excellence for Nanoscale BioPhotonics (CNBP), Australia.
E-mail address: sabrina.heng@adelaide.edu.au (S. Heng).

https://doi.org/10.1016/j.snb.2018.01.198
0925-4005/

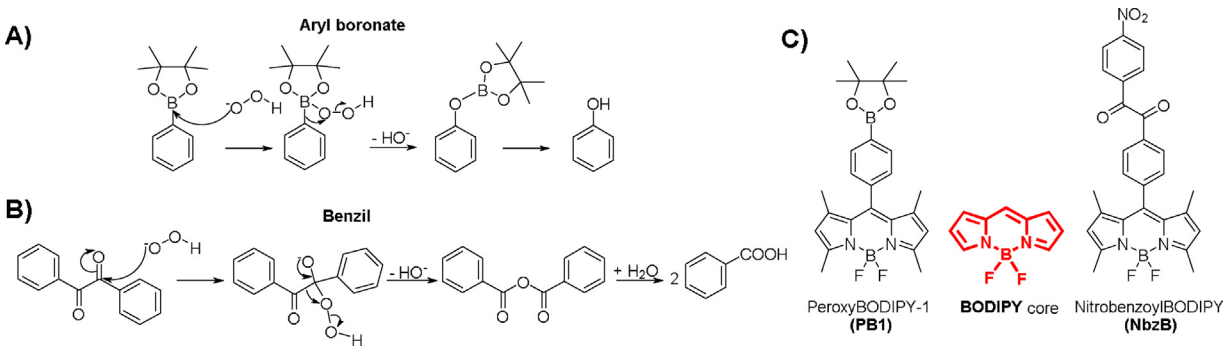

Fig. 1. New probes for detecting H_2O_2 and reaction mechanisms with H_2O_2. A) Reaction mechanism of H_2O_2 with an aryl boronate [8,13] and B) benzil [14]. C) Fluorescent probes for H_2O_2 synthesised for this study, aryl boronate **PB1** and benzil **NbzB**, shown with BODIPY core fluorescent structure.

general, the probe should 1) be biocompatible *i.e.* excellent aqueous solubility and function at physiological pH; 2) be cell permeable without the need for further chemical modifications; 3) have high selectivity for H_2O_2 over other biologically relevant species; and 4) be photostable under typical confocal microscopy experiment conditions *i.e.* minimal photobleaching when exposed to laser light from the confocal microscope.

Existing fluorescein-based aryl boronate and benzil probes [10,13], are known to have relatively poor photostability at higher concentrations of H_2O_2 where fluorescein was found to photobleach rapidly [14]. The overall measured change in fluorescence from the fluorescein-based probe may not then reflect the true concentration of H_2O_2, and thus would not be ideal for a comparative study. In contrast, the boron-dipyrromethene (BODIPY) fluorescent core structure is known to have improved photostability compared to fluorescein and properties such as biocompatibility and spectroscopic properties can be readily tuned with minor structural modifications [15].

Two new probes, peroxyBODIPY-1 (**PB1**) and nitrobenzoyl-BODIPY (**NbzB**) (Fig. 1**C**) are reported here to allow a direct comparison of aryl boronate and benzil-based detection of H_2O_2. The H_2O_2-sensitive boronate (Fig. 1**A**) and para-nitrophenyl diketone (Fig. 1**B**) groups were attached at analogous positions from the BODIPY core for both of **PB1** and **NbzB**, respectively. This study investigates the sensitivity and selectivity of **PB1** and **NbzB** to H_2O_2 and applies both to use in bovine oocytes. The utility of the aryl boronate and benzil probes is here directly compared *in vitro*, to give a clear insight into the class of probe that should be chosen for detecting H_2O_2 in biological environments.

2. Experimental

2.1. Materials and general procedures

All reagents were purchased from Sigma-Aldrich unless otherwise stated. Tetrahydrofuran (THF) was purchased from Scharlau and dried using an Innovative Technology Pure-Solv solvent purification system. Davsil silica gel (40–63 μm) was used for column chromatography. ^{1}H and ^{13}C NMR spectra were recorded in $CDCl_3$ (Cambridge Isotope Laboratories, Cambridge, MA) at 26 °C on an Agilent Technologies 500 MHz NMR with DD2 console, then analysed using Bruker TopSpin 3.2. FTIR spectra were recorded using a Perkin Elmer Spectrum 400 FT-IR/FT-FIR Spectrometer. High resolution mass spectrometry (HRMS) samples were recorded using an Agilent 6230 TOF LC–MS. All analytical reverse-phase HPLC was performed using an Agilent 1260 Infinity Analytical HPLC, using a Phenomenex Luna 5 μm C18(2) 100 Å column. Samples were run in a gradient of 10–100% acetonitrile in water over 15 min. Bovine IVF medium was prepared using VitroFert from IVF Vet Solutions (Adelaide, Australia); 4 mg/ml fatty acid free BSA (ICPBio Ltd; Auckland, New Zealand); 10 IU/ml heparin, 25 μM penicillamine, 12.5 μM hypotaurine and 1.25 μM epinephrine. *E. Coli* lipids were purchased from Avanti Polar Lipids (Alabaster, AL, USA).

2.2. Synthetic procedures

2.2.1. Compound 3

(Synthesised as per literature [16]) 4-Iodobenzoic acid (496 mg, 2 mmol) was dissolved in anhydrous $CHCl_3$ (20 mL) under an argon atmosphere. Thionyl chloride (4 mL) was added whilst stirring and the resultant solution was refluxed for 1 h. The reaction mixture was evaporated to dryness to produce crude 4-iodobenzoyl chloride, which was used without further purification. Crude 4-iodobenzoyl chloride was dissolved in $CHCl_3$ (25 mL), and 2,4-dimethylpyrrole (412 μL, 4 mmol) was added under N_2 and the reaction mixture was stirred at room temperature for 3 days. Triethylamine (1.5 mL) and $BF_3.Et_2O$ (2 mL) were added dropwise and the solution was stirred for a further 24 h. The crude product was eluted through a silica column using 3:1 PET ether/$CHCl_3$ to afford **3** as an orange solid (298 mg, 33%) **^{1}H NMR** ($CDCl_3$, 500 MHz): δ(ppm) 7.84 (2H, d, J = 8.0 Hz), 7.04 (2H, d, J = 7.5 Hz), 5.99 (2H, s), 2.55 (6H, s), 1.41 (6H, s).

2.2.2. Compound 5

BODIPY phenyl iodide **3** (42 mg, 0.095 mmol), 4-nitroethynyl benzene (17 mg, 0.11 mmol), $PdCl_2(PPh_3)_2$ (4.5 mg, 0.006 mmol) and copper (I) iodide (3 mg, 0.015 mmol) were placed in a dry vial in an inert N_2 glovebox. Triethylamine (0.1 mL) and THF (3 mL) were added and stirred overnight. The reaction mixture was then evaporated to dryness, then purified by eluting through a silica column with 2:1 PET ether/$CHCl_3$ to afford an orange solid, **5** (43 mg, 96%) **^{1}H NMR** ($CDCl_3$, 500 MHz): δ(ppm) 8.24 (2H, d, J = 8.5 Hz), 7.71–7.69 (4H, d, J = 7.5 Hz), 7.34 (2H, d, J = 8.0 Hz), 6.00 (2H, s), 2.56 (6H, s), 1.43 (6H, s). **^{13}C NMR** ($CDCl_3$, 125 MHz): δ(ppm) 156.0, 147.2, 142.9, 140.3, 136.1, 132.5, 132.3, 131.1, 129.7, 128.5, 123.7, 123.0, 121.4, 93.7, 88.7, 14.6 (t, J = 10 Hz), 14.6. **HRMS**: [M+H] calculated 471.1930, found 471.1956. **IR** (dry film) ν_{max}: 2921 (CH, aliphatic), 2220 (—C≡C—), 1593, 1539, 1508 (C=C), 1468, 1436, 1405, 1370, 1339, 1302, 1187, 1158, 1079, 1047, 971, 854, 833, 810, 765, 748, 704.

2.2.3. PeroxyBODIPY-1 (PB1)

BODIPY phenyl iodide **3** (54 mg, 0.12 mmol), bis(pinacolato)diboron (121 mg, 0.48 mmol), potassium acetate (107 mg, 1.12 mmol) and $Pd(dppf)_2Cl_2$ (10.5 mg, 0.013 mmol) were combined in a heavy-walled microwave reaction vial. The solution was dissolved in dry DMF (2 mL) and sealed with a Teflon cap in an inert N_2 atmosphere. The vial was heated under microwave

irradiation at 100 °C for 2 h. The resultant dark brown solution was poured into saturated sodium bicarbonate (15 mL), and extracted with DCM (15 mL, 2 × 10 mL). The combined organic layers were dried over $MgSO_4$ and solvent removed under reduced pressure. The crude product was eluted through a silica column using 1:1 PET ether/$CHCl_3$ to afford **PB1** as a light orange solid (54 mg, 48%). ^{1}**H NMR** ($CDCl_3$, 500 MHz): δ(ppm) 7.90 (2H, d, J = 7 Hz), 7.29 (2H, d, J = 7 Hz), 5.96 (2H, s), 2.55 (6H, s), 1.38 (12H, s), 1.36 (6H, s). ^{13}**C NMR** ($CDCl_3$, 125 MHz): δ(ppm) 155.5, 143.2, 141.6, 137.9, 135.4, 131.2, 127.3, 121.2, 84.15, 25.0, 14.6 (t, J = 10 Hz), 14.5. **HRMS-ESI**: [M+H] calculated 451.2539, found 451.2521. **IR** (dry film) ν_{max}: 2978 (CH, aliphatic), 1543, 1511 (C=C), 1470, 1398, 1360, 1307, 1260, 1194, 1157, 1144, 1084, 982, 858, 835, 719. **HPLC** retention time 25.1 min; purity 94%.

2.2.4. NitrobenzoylBODIPY (NbzB)

Alkyne **5** (24 mg, 0.051 mmol) and $PdCl_2$ (1 mg, 5.6 μmol) were dissolved in DMSO (0.5 mL) and heated to 145 °C for 4 h. The solvent was removed under reduced pressure, and the crude solid was purified by eluting through a silica column using 1:1 PET ether/$CHCl_3$ to afford an orange powder, **NbzB** (14 mg, 55%) ^{1}**H NMR** ($CDCl_3$, 500 MHz): δ(ppm) 8.39 (2H, d, J = 8.0 Hz), 8.23 (2H, d, J = 8.5 Hz), 8.15 (2H, d, J = 8 Hz), 7.53 (2H, d, J = 8 Hz), 6.01 (2H, s), 2.56 (6H, s), 1.38 (6H, s) ^{13}**C NMR** ($CDCl_3$, 125 MHz): δ(ppm) 191.6, 191.2, 156.5, 151.3, 142.6, 142.5, 139.1, 137.1, 132.7, 131.1, 130.7, 129.4, 124.2, 121.7, 14.6, 14.6 (t, J = 9.6 Hz). **MS**: [M+H] calculated 503.18, found 503.17. **IR** (dry film) ν_{max}: 2920, 2851 (CH, aliphatic), 1712, 1676 (C=O, ketone), 1544, 1519 (C=C), 1408, 1406, 1346, 1307, 1195, 1157, 1084, 982, 897, 833, 776, 738, 709. **HPLC** retention time 23.0 min; purity 95%.

2.2.5. Calibration of PB1 and NbzB with H_2O_2

A stock solution of approximately 100 mM H_2O_2 in Milli-Q water was prepared from a 30% H_2O_2 solution in water and the exact concentration was determined by UV absorption at 240 nm (ε_{240} = 43.6 M^{-1} cm^{-1}) in a quartz cuvette using a Cary UV–vis-NIR 5000 Spectrophotometer. **PB1** and **NbzB** were separately added to a 96-well plate in 100 mM phosphate buffer at pH 7.4 to give a final concentration of 10 μM of each probe. Samples were treated with 0, 5, 10, 25, 50, 75 or 100 μM of H_2O_2 in a 96-well plate. The resultant absorption and/or fluorescent spectra were monitored using a Biotek Synergy H4 fluorescence plate reader (fluorescence excitation 490 nm) over 50 min. All experiments were performed in triplicate and the results averaged.

2.2.6. ROS selectivity study

Solutions of **PB1** and **NbzB** in 100 mM phosphate buffer at pH 7.4 were treated with 100 μM of ROS: H_2O_2, $ONOO^-$, ^-OCl, $^\bullet OH$, $O_2^{\bullet-}$, NO, and *tert*-butyl hydroperoxide (TBHP). A stock solution of approximately 100 mM H_2O_2 in Milli-Q water was prepared from a 30% H_2O_2 solution in water and the exact concentration was determined by UV absorption at 240 nm (ε_{240} = 43.6 M^{-1} cm^{-1}) using a Cary UV–vis-NIR 5000 Spectrophotometer. A stock solution of NaOCl was similarly prepared and the ^-OCl concentration determined by UV absorption at 292 nm (ε_{292} = 350 M^{-1} cm^{-1}). A solution of $ONOO^-$ was prepared by a known method [17], and its concentration determined using UV absorption at 302 nm (ε_{302} = 1670 M^{-1} cm^{-1}). $^\bullet OH$ was produced by the Fenton reaction of 100 μM H_2O_2 with 1 mM $FeClO_4$. $O_2^{\bullet-}$was also produced by a known method [18], using a xanthine/xanthine oxidase system for production of $O_2^{\bullet-}$ and catalase as a scavenger for any H_2O_2 produced. NO was generated from S-nitrosoglutathione, and TBHP was diluted from a stock solution. The ROS were added to each probe and the fluorescence was monitored using a Biotek Synergy H4 fluorescence plate reader (excitation 490 nm, emission 510 nm) over 50 min. All experiments were performed in triplicate and the results averaged.

2.2.7. Density functional theory calculations

Three initial structures were created in Avogadro [19]; **PB1**, **6**, and **NbzB** and subjected to a preliminary molecular mechanics optimisation using a steepest-descent strategy and the MMFF94 [20] force field, for at least 500 steps. The resulting structures were used to create input position files for *ab initio* density functional theory calculations in the Vienna *ab initio* simulation package (VASP) [21].

The VASP calculations used plane-augmented wave pseudopotentials [22,23], the PBE [24] generalised-gradient approximation exchange-correlation functional, a plane-wave cutoff energy of ~16,000 kcal/mol (700 eV), and k-point sampling at the Γ point only. The structures were geometry optimised in VASP until their free energies converged to <2.3 cal/mol and the maximum force on any one atom was below 230 cal/mol $Å^{-1}$. Single-step calculations for accurate total energies and extraction of the HOMO and LUMO electron densities were then carried out, converged to 23 mcal/mol.

Fig. 3 and Fig. S3 (Supplementary Information) were made using VESTA [25].

2.2.8. Preparation of NbzB liposomes

The liposomes were generated by dissolving **NbzB** in DMSO (8 mg/ml) and mixing it with a solution containing 25 mg of *E. Coli* total lipid extract in 1 mL buffer (20 mM MOPS, 5% maltose, pH 7.2). Large multi-lamellar liposomes were formed by sonication and vortexing of the lipid-**NbzB** mixture for 60 min. The lipid-**NbzB** mixture was clarified to remove unincorporated insoluble **NbzB** by high-speed centrifugation at 15,000 × g for 20 min at room temperature followed by ultracentrifugation at 120,000 × g for 60 min at 25 °C to isolate the liposome fraction. The lipid pellet containing the liposomes was washed twice with buffer (1 mL) to remove any soluble **NbzB** and then resuspended in buffer (1 mL). Uni-lamellar **NbzB** liposomes were generated by extruding the mixture through a 0.2 μm membrane. After 11 passages **NbzB** liposomes with a median diameter of 180 nm were generated for analysis.

Liposomes were then treated with H_2O_2 (100 μM) and incubated at 25 °C for 10 min. The fluorescence was then recorded using a Biotek Synergy H4 fluorescence plate reader (fluorescence excitation 490 nm).

2.2.9. Detection of H_2O_2 in bovine oocytes

Bovine oocytes were denuded of cumulus cells after 24 h *in vitro* maturation at 38 °C in standard culture conditions [9]. Half of the oocytes were treated with 1 mM H_2O_2 and then incubated for a further 30 min. Oocytes were then transferred to solutions containing either **PB1** or **NbzB** at a concentration of 10 μM in wash medium (VitroWash + 4 mg/ml fatty acid free BSA). Oocytes were then incubated for 30 min, briefly washed in wash medium and transferred into 5 μL drops of wash medium in glass-bottom confocal dishes (Cell E&G; Houston, TX). These droplets were overlaid with oil and the fluorescence from each oocyte was captured using a FluoView FV10i confocal microscope and accompanying software (Olympus; Tokyo, Japan). Both **PB1** and **NbzB** were measured using 490 nm excitation and 509 nm emission filters. Microscope settings, including laser intensity, aperture and image size were kept constant while imaging. Quantification of the fluorescence was calculated using ImageJ software (National Institutes of Health, Bethesda, MD). The fluorescence intensity across the diameter of the oocyte was calculated, and an average for each treatment group is presented in Fig. S4. Representative graphs and images are presented in Fig. 5.

Other experimental procedures such as determination of reaction rates, quantum yields and toxicity studies with HEK293 cells can be found in the Supplementary Information section.

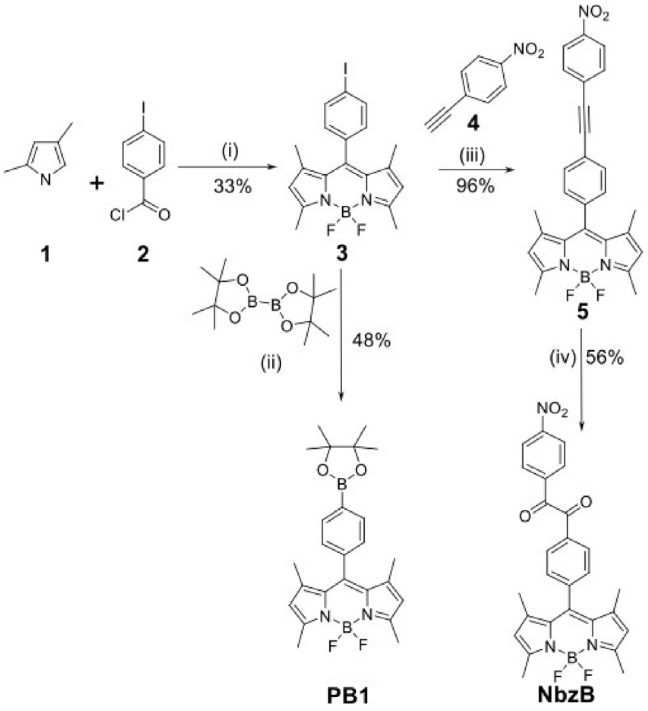

Scheme 1. Synthesis of BODIPY-based H_2O_2 sensors. (i) 1. Chloroform, room temperature (r.t.), 72 h; 2. Triethylamine (Et_3N), Boron trifluoride diethyl etherate, r.t., 24 h. (ii) $Pd(dppf)Cl_2$, potassium acetate, dimethylformamide (DMF), 100 °C, 2 h. (iii) $PdCl_2(PPh_3)_2$, copper iodide, Et_3N, tetrahydrofuran (THF), r.t., 16 h. (iv) $PdCl_2$, dimethyl sulfoxide (DMSO), 145 °C, 4 h.

3. Results and discussion

3.1. Synthesis

PB1 and **NbzB** were synthesized from common intermediate (**3**), which was readily prepared on reaction of 2,4-dimethylpyrrole **1** with 4-iodobenzoic acid **2**, see Scheme 1. Reaction of **3** with bis(pinacolato)diboron under Suzuki conditions gave **PB1** in a 48 % yield. Alternately, reaction of intermediate **3** with 4-ethynyl-1-nitrobenzene **4**, under Sonigashira conditions, gave **5** as an immediate precursor to **NbzB**. The alkyne functionality on compound **5** was oxidised with DMSO and $PdCl_2$ to give **NbzB** in 54% yield over two steps from intermediate **4**.

3.2. Spectroscopic analysis of PB1 and NbzB with H_2O_2

The first part of the study involved a comparison of the responses of **PB1** and **NbzB** to H_2O_2 to determine their respective sensitivity and selectivity. **PB1** was reacted with five different concentrations of H_2O_2 (ranging from 5 to 100 μM) and the fluorescent responses were measured after 50 min. The resultant plots shown in Fig. 2**A** clearly reveal that fluorescence quenches with increasing H_2O_2, because of the reaction between aryl boronate and H_2O_2 to form the phenol (**6**). The quantum yield of **PB1** in the presence of H_2O_2 (100 μM) was determined to be 0.024 using fluorescein as the calibration standard (see Supplementary Information Fig. S5B). While, the lower level of detection of H_2O_2 observed for **PB1** (5 μM) is consistent with reports on other aryl boronate probes [26], **PB1** differs from previously reported probes [8] with fluorescence quenching on reaction with H_2O_2. The absorption spectrum of **PB1** was measured over the course of the above experiment to gain further insights into the emission quenching. Unlike fluorescence emission, the absorption spectrum remained unchanged for all concentrations of H_2O_2 (see Supplementary Information, Fig. S1). This similar

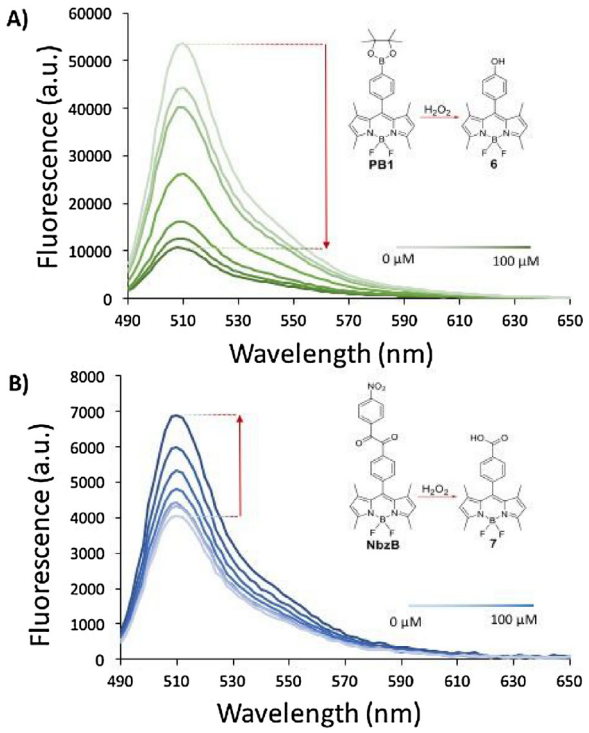

Fig. 2. Response of **PB1** and **NbzB** to 0, 5, 10, 25, 50, 75 and 100 μM of H_2O_2 over 50 min in 100 mM phosphate buffer at pH 7.4. (A) Decrease in fluorescent spectra of **PB1** when incubated with H_2O_2 (excitation 470 nm). **PB1** is oxidized by H_2O_2 to give the alcohol **6** as shown. (B) Increase in fluorescent spectra of **NbzB** when incubated with H_2O_2 (excitation 470 nm). **NbzB** is oxidized by H_2O_2 to give the acid **7** as shown. Emission wavelengths for **6** and **7** were determined to be 510 nm respectively.

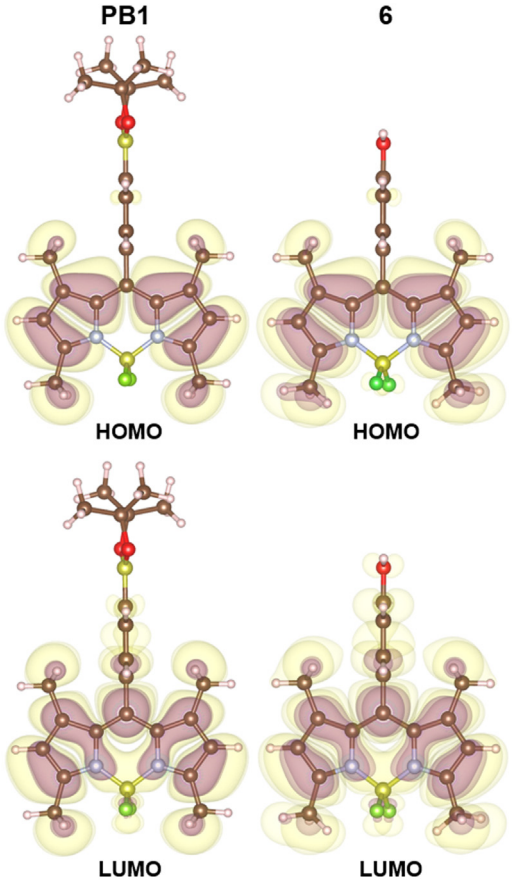

Fig. 3. Calculated electron densities of HOMO and LUMO of **PB1** and **6**.

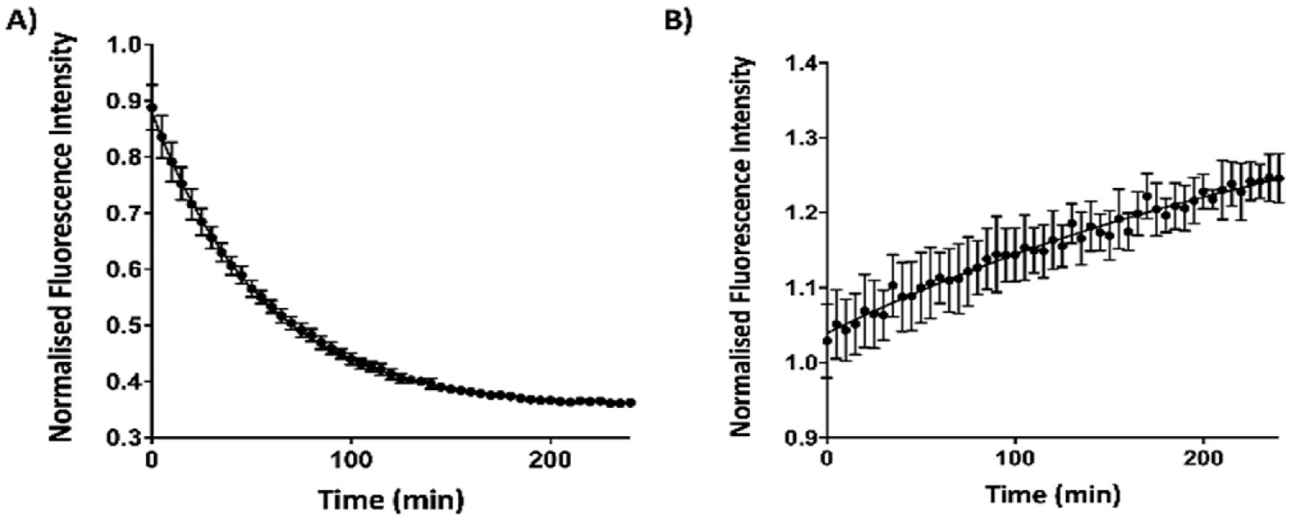

Fig. 4. Time-dependent fluorescence decay or increase curves after the addition of H_2O_2 (100 μM) for A) **PB1** and B) **NbzB** in 1% DMSO in water. Recording interval: 5 min. Curve (R^2 = 0.98 for **PB1** and 0.87 for **NbzB**) was obtained using GraphPad Prism 7.0.

absorption of **PB1** and **6** was further confirmed by calculating the electron densities of the HOMO and LUMO states of both **PB1** and its product **6** by density functional theory. An analysis revealed that the energy gap between HOMO and LUMO states of **PB1** and **6** were comparable (44.2 kcal mol^{-1} and 44.5 kcal mol^{-1} respectively). This is consistent with **PB1** and its product upon reaction with H_2O_2 (**6**) exhibiting the same absorption spectra (Fig. S1). Furthermore, the HOMO of both **PB1** and **6** (Fig. 3) show π-character delocalised across the BODIPY core only, with little electron density on the perpendicular phenyl ring, for both **PB1** and **6**. However, the LUMO of **6** has less electron density across the BODIPY core compared to **PB1**, with more density on the perpendicular phenyl ring, presumably due to the electronegative phenol. The enhanced electron density in the phenyl π-system and corresponding decrease in the fluorescent BODIPY core, is consistent with the excited electrons in **6** being less likely to emit a photon when transitioning back to the ground state, compared to **PB1**. This computational result hence supports the assertion that the observed decrease in fluorescence is the result of **PB1** reacting with H_2O_2 to give **6**, rather than a degradation of the BODIPY fluorescent core.

In contrast to **PB1**, the fluorescence increase for the benzil-based sensor (**NbzB**) is proportional to increasing concentrations of H_2O_2 (from 5 μM to 100 μM) as shown in Fig. 2**B**. Again, **NbzB** was sensitive to at least 5 μM H_2O_2, which is consistent with limits of other fluorescein-based benzil probes [10]. **PB1** exhibits a greater change in fluorescence upon reaction with H_2O_2, with a >5-fold decrease in fluorescence on incubation with 100 uM H_2O_2 (Fig. 2A). Interestingly, the excitation (Ex) and emission (Em) wavelengths for both **PB1** and **NbzB** and the associated products, **6** and **7** were determined to be Ex = 470 nm and Em = 510 nm respectively (see Fig. 2). The aryl boronate and benzyl substituents were not observed to affect the peak wavelengths, which is consistent with the absorption profiles and electron density calculations. In comparison, **NbzB** presents approximately 1.75-fold increase in fluorescence at the same concentration of H_2O_2 (Fig. 2**B**). The quantum yield of **NbzB** in the presence of H_2O_2 (100 μM) was determined to be 0.020 using fluorescein as the calibration standard (see Supplementary Information Fig. S5A). It was initially uncertain if the solubility of **NbzB** in buffer affected this fluorescence response. To address this potential issue, an alternate means of dissolution was used by embedding **NbzB** in the membrane of liposomes prepared from *E. Coli* total lipids, a technique that aids in solubilising hydrophobic fluorophores [27]. The liposomal preparation was then treated with H_2O_2 and the resultant fluorescence recorded (Supplementary Information, Fig. S2). The fluorescent response shown by **NbzB** embedded in liposomes was an identical 1.75-fold increase. This suggested that **NbzB** retains its ability to detect H_2O_2 when embedded in liposomes and thus the solubility of **NbzB** was not affecting its fluorescent response. The increase in fluorescence upon reaction with H_2O_2 was explored further by calculating the electron densities of the HOMO and LUMO states of **NbzB** using density functional theory (see Supplementary Information, Fig. S3). Although the HOMO of **NbzB** is very similar to **PB1** (Fig. 3), with delocalised π-systems across the fluorescent BODIPY

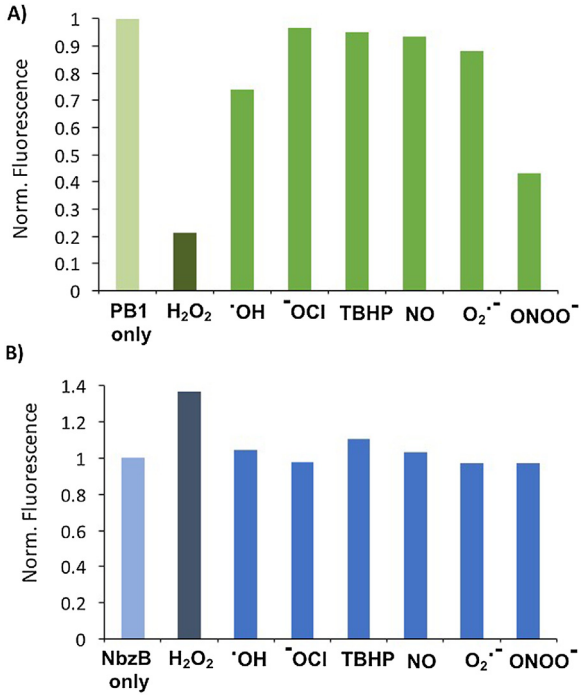

Fig. 5. Responses of **PB1** and **NbzB** to: H_2O_2, hydroxyl radicals (•OH), hypochlorite ($^-$OCl), tert-butyl hydroperoxide (TBHP), nitric oxide (NO), superoxide ($O_2^{\bullet -}$) and peroxynitrite ($ONOO^-$). Samples were exposed to 100 μM ROS over 40 min in 100 mM phosphate buffer at pH 7.4. Excitation was set at 470 nm, and emission was collected at 510 nm. (A) Fluorescent quenching of **PB1** when incubated with 100 μM ROS. (B) Fluorescent increase of **NbzB** when incubated with 100 μM ROS.

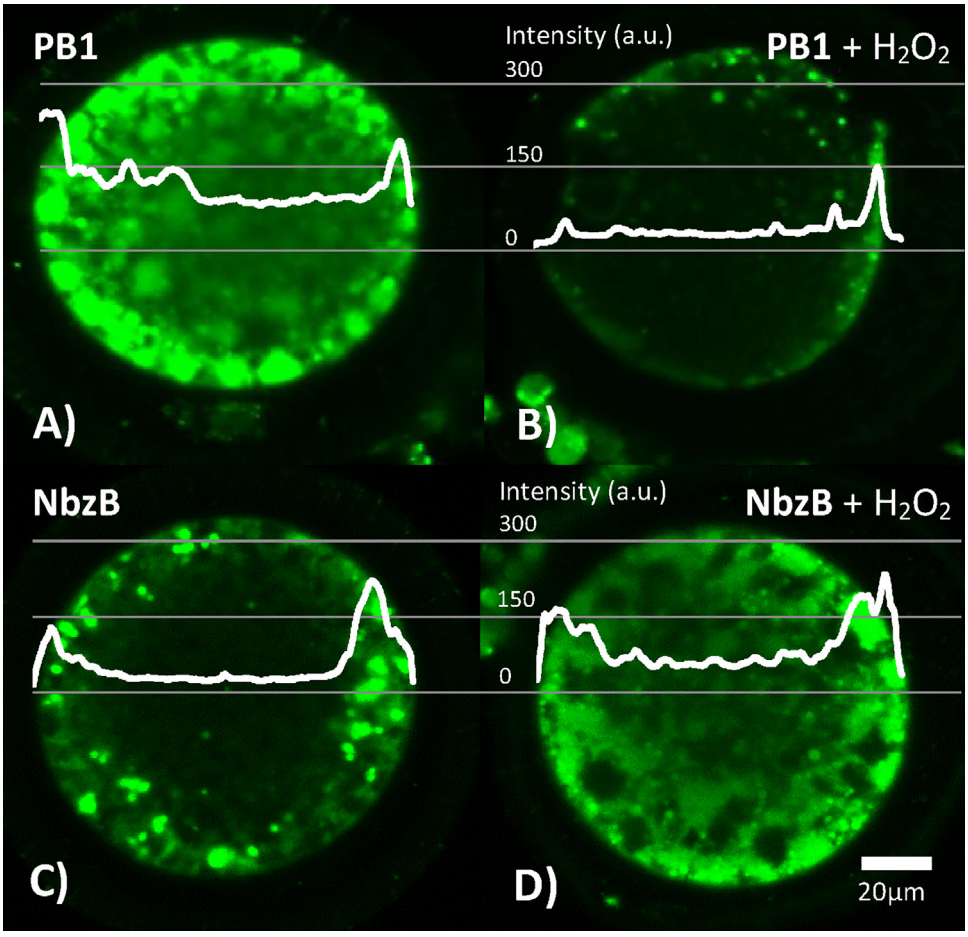

Fig. 6. Representative confocal microscope images of denuded bovine oocytes stained with **PB1** and **NbzB** (exc. 490 nm, em. 509 nm). The intensity of fluorescence across the diameter of each oocyte is plotted for comparison. A) **PB1** stain in absence of H_2O_2. B) **PB1** stain after H_2O_2 treatment. C) **NbzB** stain in absence of H_2O_2. D) **NbzB** stain after H_2O_2 treatment.

core, the LUMO instead exhibited electron density solely across the para-nitrophenyl diketone group and its corresponding phenyl that are shown perpendicular to the BODIPY core (Fig. S3). These calculations suggest the lower initial fluorescence of **NbzB** is due to the expected energy transfer to this adjacent para-nitrophenyl group upon excitation, which is cleaved after reacting with H_2O_2. Hence, the observed increase in fluorescence upon reaction with H_2O_2 is confirmed by DFT calculation.

Finally, the time-dependent fluorescence decay or increase of **PB1** or **NbzB** in the presence of H_2O_2 (100 μM) were measured at room temperature in 1% DMSO/water to approximate the reaction rate for this reaction. The decrease or increase in fluorescence was measured at 5 min intervals upon addition of H_2O_2, and the results are shown in Fig. 4. The reaction for **PB1** is well approximated by a single exponential decay ('turn-off') to give an observed rate constant of 0.018 s^{-1} and half-life of 38 min (Fig. 4**A**). The reaction was complete after 200 min. In contrast, the reaction between **NbzB** and H_2O_2 was found to be slower under similar experimental conditions (Fig. 4**B**). However, an accurate half-life and K_{obs} could not be determined for **NbzB** using this method due to the small change in fluorescence upon reaction with H_2O_2. Further work is required to fully characterize the kinetics of both reactions, but it is important to note that the observed reaction rate between **PB1** and H_2O_2 is within the time-scale of recently reported ROS sensors [28,29].

3.3. Selectivity profiles of PB1 and NbzB

The selectivity of **PB1** to a range of other ROS [hydroxyl radicals ($^{\bullet}OH$), hypochlorite (^{-}OCl), tert-butyl hydroperoxide (TBHP), nitric oxide (NO), superoxide ($O_2^{\bullet-}$) and peroxynitrite ($ONOO^-$)] was next investigated. Each ROS (100 μM) was incubated with separate samples of **PB1** and the resultant fluorescent responses measured. The results shown in Fig. 5**A** clearly show that **PB1** is more sensitive to H_2O_2 compared to the other six ROS, with some decrease in fluorescence observed for $ONOO^-$ and $^{\bullet}OH$ but not ^{-}OCl, TBHP, NO and $O_2^{\bullet-}$. Thus, **PB1** has good selectivity for H_2O_2 over most ROS with the exception of a lesser reaction with $^{\bullet}OH$ and also $ONOO^-$, which is consistent with literature [30].

The selectivity profile of **NbzB** toward the before-mentioned range of ROS ($^{\bullet}OH$, ^{-}OCl, TBHP, NO, $O_2^{\bullet-}$ and $ONOO^-$) was investigated by incubating with 100 μM solutions of each analyte and measuring the resultant change in fluorescence maximum (see Fig. 5**B**). Little difference in fluorescence was apparent for samples incubated with $^{\bullet}OH$, ^{-}OCl, TBHP, NO, $O_2^{\bullet-}$ and $ONOO^-$ compared to the control. Thus, although showing a modest increase in fluorescence, **NbzB** shows a higher selectivity for H_2O_2 than **PB1**. This observation is supported by literature, which suggests that benzil-based probes [10,11] possess selectivity for H_2O_2 that is more exclusive of other ROS than do aryl boronates [30]. Benzil-based probes such as **NbzB** are therefore well suited to applications where a high degree of selectivity for H_2O_2 is required.

3.4. Cell studies

Next HEK 293 cells were separately incubated with 1 μM, 5 μM, 10 μM and 50 μM of each sensor for up to 48 h to examine and compare the effect of each sensor on cell proliferation, as determined by Neutral Red assay (Fig. S6) [31]. The longer incubation times, particularly above 24 h, are important for determining the toxicity of the sensor with prolonged incubation. The results in the corresponding Supplementary Information section show that concentrations up to 5 μM of both sensors do not affect cell proliferation significantly. This is consistent with literature findings on the general toxicity of BODIPY-based sensors [28,32].

Finally, the ability of **PB1** and **NbzB** to detect H_2O_2 were assessed *in vitro* with bovine oocytes. Both gametes (sperm and oocytes) and early embryos are particularly sensitive to ROS attack [33] and levels of ROS, including H_2O_2, during *in vitro* manipulation are found in higher levels than within *in vivo*-derived gametes and embryos. High levels of ROS are associated with an increased incidence of DNA damage and reduced viability. Commercially available BODIPY-based fluorophores, such as H_2DCFDA, are frequently used to examine ROS levels in gametes and embryos [4], but are not specific for H_2O_2. Furthermore, oocytes are known to be poorly permeable toward fluorophores and thus this experiment provides an opportunity to explore cell-permeability and detection of H_2O_2 in cells. Oocytes were denuded of cumulus cells following *in vitro* maturation and incubated in the absence or presence of 1 mM H_2O_2 for 30 min at 38 °C. The oocytes were washed and then stained with either **PB1** or **NbzB** and incubated for a further 30 min. The oocytes were imaged by confocal microscopy, with representative results shown in Fig. 6 (see Supplementary Information for population average, Fig. S4). The fluorescence of both **PB1** and **NbzB** are clearly shown with the cells, and thus each have permeated into the oocytes. The intensity of fluorescence decreased significantly when cells were treated with H_2O_2 (Fig. 6**B**). Conversely, oocytes stained with **NbzB** only showed a minor increase in fluorescence when treated with H_2O_2 (Fig. 6**C** and **D**). Thus, **PB1** is more sensitive to H_2O_2 than **NbzB** in cells.

4. Conclusions

PB1 and **NbzB** were synthesised from a common intermediate BODIPY. These probes were compared to determine the respective sensitivity and selectivity of the aryl boronate and benzil groups to H_2O_2. **PB1** showed higher sensitivity to H_2O_2 than did **NbzB**, with a greater fluorescent response. **PB1** also showed a good fluorescent response to H_2O_2 in bovine oocytes. Despite less sensitivity to H_2O_2, **NbzB** was more selective for H_2O_2 over other ROS than **PB1**. Hence it is advantageous to utilise benzils to distinguish H_2O_2 where $ONOO^-$ or $^{\bullet}OH$ are also present. The results from this crucial experimental comparison should encourage caution when life scientists are choosing probes for H_2O_2, as aryl boronates and benzils must be used in parallel to thoroughly characterise H_2O_2 production in cellular environments.

Acknowledgements

This research was supported in part by Cook Medical Pty Ltd, Australian Research Council linkage grant LP110200736, and the ARC Centre of Excellence for Nanoscale BioPhotonics (CNBP)CE140100003. This work was performed in part at the Opto-Fab node of the Australian National Fabrication Facility (ANFF) utilizing Commonwealth and SA State Government funding. This research was also undertaken in part on the NCI National Facility in Canberra, Australia, which is supported by the Australian Commonwealth Government. The authors acknowledge Robyn Louise Kievit for performing the cytotoxicity studies.

Appendix A. Supplementary data

Supplementary data associated with this article can be found, in the online version, at https://doi.org/10.1016/j.snb.2018.01.198.

References

[1] S.G. Rhee, T.S. Chang, W. Jeong, D. Kang, Methods for detection and measurement of hydrogen peroxide inside and outside of cells, Mol. Cells 29 (2010) 539–549.
[2] G. Groeger, C. Quiney, T.G. Cotter, Hydrogen peroxide as a cell-survival signaling molecule, Antioxid. Redox Signaling 11 (2009) 2655–2671.
[3] R.J. Aitken, B.J. Curry, Redox regulation of human sperm function: from the physiological control of sperm capacitation to the etiology of infertility and DNA damage in the germ line, Antioxid. Redox Signaling 14 (2011) 367–381.
[4] S. Morado, P. Cetica, M. Beconi, J.G. Thompson, G. Dalvit, Reactive oxygen species production and redox state in parthenogenetic and sperm-mediated bovine oocyte activation, Reproduction 145 (2013) 471–478.
[5] M.L. Sutton-McDowall, L.L. Wu, M. Purdey, A.D. Abell, E.M. Goldys, K.L. MacMillan, et al., Nonesterified fatty acid-induced endoplasmic reticulum stress in cattle cumulus oocyte complexes alters cell metabolism and developmental competence, Biol. Reprod. 94 (2016) 23.
[6] M.L. Sutton-McDowall, M. Purdey, H.M. Brown, A.D. Abell, D.G. Mottershead, P.D. Cetica, et al., Redox and anti-oxidant state within cattle oocytes following in vitro maturation with bone morphogenetic protein 15 and follicle stimulating hormone, Mol. Reprod. Dev. 82 (2015) 281–294.
[7] M.S. Purdey, H.S. Connaughton, S. Whiting, E.P. Schartner, T.M. Monro, J.G. Thompson, et al., Boronate probes for the detection of hydrogen peroxide release from human spermatozoa, Free Radic. Biol. Med. 81 (2015) 69–76.
[8] A.R. Lippert, G.C. Van de Bittner, C.J. Chang, Boronate oxidation as a bioorthogonal reaction approach for studying the chemistry of hydrogen peroxide in living systems, Acc. Chem. Res. 44 (2011) 793–804.
[9] V.S. Lin, B.C. Dickinson, C.J. Chang, Boronate-based fluorescent probes: imaging hydrogen peroxide in living systems, Methods Enzymol. 526C (2013) 19–43.
[10] M. Abo, Y. Urano, K. Hanaoka, T. Terai, T. Komatsu, T. Nagano, Development of a highly sensitive fluorescence probe for hydrogen peroxide, J. Am. Chem. Soc. 133 (2011) 10629–10637.
[11] M. Abo, R. Minakami, K. Miyano, M. Kamiya, T. Nagano, Y. Urano, et al., Visualization of phagosomal hydrogen peroxide production by a novel fluorescent probe that is localized via SNAP-tag labeling, Anal. Chem. 86 (2014) 5983–5990.
[12] C.C. Winterbourn, Reconciling the chemistry and biology of reactive oxygen species, Nat. Chem. Biol. 4 (2008) 278–286.
[13] M.C.Y. Chang, A. Pralle, E.Y. Isacoff, C.J. Chang, A selective, cell-permeable optical probe for hydrogen peroxide in living cells, J. Am. Chem. Soc. 126 (2004) 15392–15393.
[14] M. Platkov, R. Tirosh, M. Kaufman, N. Zurgil, M. Deutsch, Photobleaching of fluorescein as a probe for oxidative stress in single cells, J. Photochem. Photobiol. B 140 (2014) 306–314.
[15] A. Loudet, K. Burgess, BODIPY dyes and their derivatives: syntheses and spectroscopic properties, Chem. Rev. 107 (2007) 4891–4932.
[16] R. Ziessel, G. Ulrich, A. Haefele, A. Harriman, An artificial light-harvesting array constructed from multiple Bodipy dyes, J. Am. Chem. Soc. 135 (2013) 11330–11344.
[17] S.L. Hempel, G.R. Buettner, Y.Q. O'Malley, D.A. Wessels, D.M. Flaherty, Dihydrofluorescein diacetate is superior for detecting intracellular oxidants: comparison with 2' 7'-dichlorodihydrofluorescein diacetate, 5 (and 6)-carboxy-2',7'-dichlorodihydrofluorescein diacetate, and dihydrorhodamine 123, Free Radic. Biol. Med. 27 (1999) 146–159.
[18] A.E. Albers, B.C. Dickinson, E.W. Miller, C.J. Chang, A red-emitting naphthofluorescein-based fluorescent probe for selective detection of hydrogen peroxide in living cells, Bioorg. Med. Chem. Lett. 18 (2008) 5948–5950.
[19] M.D. Hanwell, D.E. Curtis, D.C. Lonie, T. Vandermeersch, E. Zurek, G.R. Hutchinson, Avogadro: an advanced semantic chemical editor, visualization, and analysis platform, J. Cheminf. 4 (2012) 17.
[20] T.A. Halgren, Merck molecular force field. I. Basis, form, scope, parameterization, and performance of MMFF94*, J. Comput. Chem. 17 (1996) 490–519.
[21] G. Kresse, J. Furthmuller, Efficient iterative schemes for ab initio total-energy calculations using a plane-wave basis set, Phys. Rev. B 54 (1996) 11169–11186.
[22] P.E. Blöchl, O. Jepsen, O.K. Andersen, Improved tetrahedron method for Brillouin-zone integrations, Phys. Rev. B 49 (1994) 16223–16233.
[23] G. Kresse, D. Joubert, From ultrasoft pseudopotentials to the projector augmented-wave method, Phys. Rev. B 59 (1999) 1758–1775.
[24] J.P. Perdew, K. Burke, M. Ernzerhof, Generalized gradient approximation made simple, Phys. Rev. Lett. 77 (1996) 3865–3868.

[25] K. Momma, F. Izumi, VESTA 3 for three-dimensional visualization of crystal, volumetric and morphology data, J. Appl. Crystallogr. 44 (2011) 1272–1276.
[26] E.W. Miller, A.E. Albers, A. Pralle, E.Y. Isacoff, C.J. Chang, Boronate-based fluorescent probes for imaging cellular hydrogen peroxide, J. Am. Chem. Soc. 127 (2005) 16652.
[27] S. Heng, C.A. McDevitt, D.B. Stubing, J.J. Whittall, J.G. Thompson, T.K. Engler, et al., Microstructured optical fibers and live cells: a water-soluble, photochromic zinc sensor, Biomacromolecules 14 (2013) 3376–3379.
[28] J. Xu, Q. Li, Y. Yue, Y. Guo, S. Shao, A water-soluble BODIPY derivative as a highly selective Turn-On fluorescent sensor for H2O2 sensing in vivo, Biosens. Bioelectron. 56 (2014) 58–63.
[29] D. Srikun, A.E. Albers, C.J. Chang, A dendrimer-based platform for simultaneous dual fluorescence imaging of hydrogen peroxide and pH gradients produced in living cells, Chem. Sci. 2 (2011) 1156–1165.
[30] A. Sikora, J. Zielonka, M. Lopez, J. Joseph, B. Kalyanaraman, Direct oxidation of boronates by peroxynitrite: mechanism and implications in fluorescence imaging of peroxynitrite, Free Radic. Biol. Med. 47 (2009) 1401–1407.
[31] T.F. Uliasz, S.J. Hewett, A microtiter trypan blue absorbance assay for the quantitative determination of excitotoxic neuronal injury in cell culture, J. Neurosci. Methods 100 (2000) 157–163.
[32] S.O. Tümay, E. Okutan, I.F. Sengul, E. Özcan, H. Kandemir, T. Doruk, et al., Naked-eye fluorescent sensor for Cu(II) based on indole conjugate BODIPY dye, Polyhedron 117 (2016) 161–171.
[33] A. Agarwal, R.A. Saleh, M.A. Bedaiwy, Role of reactive oxygen species in the pathophysiology of human reproduction, Fertil. Steril. 79 (2003) 829–843.

Biographies

Malcolm Purdey is an Adjunct Fellow at the University of Adelaide and Associate Investigator in the ARC Centre of Excellence in Nanoscale BioPhotonics (CNBP). Malcolm obtained his PhD from the University of Adelaide in 2015 and subsequently worked in the Institute for Photonics and Advanced Sensing (IPAS) with Professor Andrew Abell. His research focuses on the application of fluorescent sensors for detecting reactive oxygen species in biological systems.

Hanna McLennan graduated from the University of Adelaide with B.Health.Sc. (Hons) in 2015 and is currently a PhD candidate within CNBP and Robinson Research Institute (RRI) under the supervision of Associate Professor Jeremy Thompson and Drs. Melanie Sutton-McDowall and Sabrina Heng. Her research has a transdisciplinary focus using tools developed by chemists and physicists within the CNBP to investigate and detect the signals produced by the oocyte during *in vitro* fertilisation.

Melanie Sutton-McDowall is an Adjunct Fellow in the Adelaide Medical School and previously was a Senior Research Associate at CNBP and the Robinson Research Institute. Dr Sutton-McDowall obtained her PhD in Health Sciences, The University of Adelaide, in 2005 and the focus of her research was how the metabolic activity of oocytes and embryos are influenced by the surrounding environment, both *in vivo* and *in vitro*.

Daniel Drumm received his Ph.D. from The University of Melbourne (2013), and is now a Research Fellow with CNBP in Physics at RMIT University. He has modelled a range of systems from semiconductor defects for quantum computation and communications, through transition metal oxides, organometallic crystals, ternary chalcogenide glasses, polymer-dye-sensitised solar cells, nuclear physics, and now fluorescent-dye-based sensors. He has also worked on a cloud-based computation system, and is currently focussing on quantum correlation imaging, transition-metal dichalcogenides, search algorithms for accelerating microscopy, and collaborating on applying modelling techniques to other systems.

Xiaozhou Zhang graduated from the University of Adelaide with B.Sc (Hon) and Ph.D. under the supervision of Professor Andrew Abell. She is currently undertaking post-doctoral research at CNBP and her research interests include developing biocompatible sensors and sensing strategies for detecting biologically-relevant substrates.

Patrick Capon graduated from the University of Adelaide with BSc (Advanced) and MPhil. in 2016 and is currently a PhD candidate within the CNBP under the supervision of Professor Andrew Abell and Dr. Malcolm Purdey. His research focuses on developing multi-component biological sensors consisting of nanodiamond and organic fluorescent probes.

Sabrina Heng is a Senior Research Associate at CNBP. Sabrina obtained her PhD from Boston College (MA, USA) in 2009. Shortly after, she joined the Institute for Photonics and Advanced Sensing (IPAS) and School of Chemistry and Physics to work with Professors Andrew Abell and Tanya Monro. In 2010, she was awarded the inaugural ARC Super Science Fellowship to develop light-driven sensors for metal ions.

Jeremy Thompson is an Associate Professor at the University of Adelaide, the Head of Early Development Group and chief investigator with the CNBP. His overall research interest is the impact of the micro-environment surrounding oocytes and embryos, especially nutritional factors, within both the *in vivo* (follicular/oviduct/uterine) and *in vitro* environment. This encompasses hypoxia, hypoxia inducible factors and their role in reproduction

Andrew Abell is a Professor of Chemistry, Adelaide node leader CNBP and is an Australian Fulbright ambassador. He completed his PhD in Chemistry at the University of Adelaide in 1985 and then a two-year post-doctoral fellowship at the University of Cambridge. He held a professorship at the University of Canterbury, before returning to Adelaide in 2007.